Millimeter-Wave FET Nonlinear Modelling Based on the Dynamic-Bias Measurement Technique

Gustavo Avolio, *Member, IEEE*, Antonio Raffo, *Member, IEEE*, Iltcho Angelov, Valeria Vadalà, *Member, IEEE*, Giovanni Crupi, *Senior Member, IEEE*, Alina Caddemi, *Member, IEEE*, Giorgio Vannini, *Member, IEEE*, and Dominique M. M.-P. Schreurs, *Fellow, IEEE*

***Abstract*—In the paper, the nonlinear model of a microwave transistor is extracted from large-signal measurements acquired under "dynamic-bias" operation. Specifically, the transistor is driven by low-frequency large signals while a high-frequency tickle is applied on top of them. The low-frequency large signals, along with the dc bias voltages, set the large-signal operating point which represents a dynamic-bias condition for the device under test. Thanks to this technique, one can get at once and separately the nonlinear currents and charges of the transistor as a result of a very few nonlinear measurements. Additionally, the proposed technique allows one to accurately reconstruct the time-domain waveforms at the device-under-test terminals while the frequency of the tickle can be set as high as the bandwidth of today's vector calibrated nonlinear measurement systems (i.e., 67 GHz). The approach, which is general and independent of device technology, is applied on a 0.15-μm GaAs pHEMT specifically designed for resistive cold-FET mixer applications.**

***Index Terms*—Dynamic-bias, field-effect transistors (FETs), nonlinear measurements, nonlinear models, semiconductor device measurements.**

I. Introduction

TYPICALLY, models of microwave transistors are described in terms of nonlinear conductive current and charge along with parasitic elements accounting for the device layout, as shown in Fig. 1. The values of the transistor nonlinear conductive currents $(\mathrm{I_G}, \mathrm{I_D})$ and charges $(\mathrm{Q_G}, \mathrm{Q_D})$ can be derived directly from measurements and either stored in lookup tables (LUTs) or represented by analytical expressions [1]–[8]. Many approaches rely on the use of dc and small-signal measurements, as shown, for example, in [3] and [6]. These measurements already provide a lot of information about the transistor currents and charges. Along with these measurements, in the last decades, nonlinear measurements have also entered the modeling phase [9], [10]. These measurements can be acquired with a large-signal network analyzer (LSNA) or a nonlinear vector network analyzer (NVNA) which enable vector calibrated nonlinear measurements. Therefore, one can acquire the actual time-domain waveforms at the transistor terminals and use them to extract the values of the currents and the charges. LSNAs and NVNAs are today available ranging from few kilohertz up to 67 GHz [11]–[13] and since many years have been heavily used for transistor nonlinear model extraction. In [7], LSNA measurements at low frequencies (LF) are used to extract the transistor conductive currents, including dispersive effects under nonlinear dynamic operation. In [1], [2], [5], [8], time-domain waveforms in the microwave range are used to extract both the conductive currents and the charges. Other approaches [14]–[16] make use of the LSNA or NVNA frequency-domain data to identify behavioral models. Obviously, approaches which rely directly on time-domain data require that the time-domain waveforms generated by a nonlinear device should be accurately measured implying the acquisition of a sufficient number of harmonic frequencies. Today's NVNA instruments enable measurements up to 67 GHz. Therefore, if one wants to acquire time-domain waveforms including at least three harmonics with a 67-GHz NVNA, the excitation frequency can be at most equal to 67 GHz divided by three.

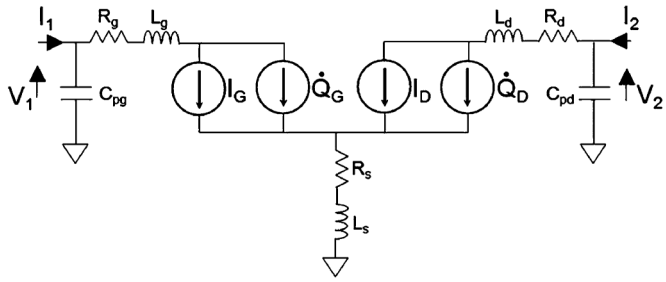

Fig. 1. Nonlinear model of a field-effect transistor (FET).

In this work, we propose an alternative approach which actually combines the capabilities of nonlinear measurement systems operating at different frequencies. This new approach is described in Section II and relies on the concept of *dynamic-bias* [17]. The main nonlinearities of the device under test (DUT) are induced by means of large signals at low frequencies in the

Manuscript received May 29, 2014; revised August 08, 2014; accepted September 06, 2014. Date of publication October 13, 2014; date of current version November 03, 2014. This work was supported by FWO—Vlaanderen (Belgium) and EMRP 'HF Circuits' project. This paper is an expanded version from the IEEE MTT-S International Workshop on Integrated Nonlinear Microwave and Millimetre-wave Circuits (INMMiC), Leuven, Belgium, 2–4 April 2014.

G. Avolio and D. M. M.-P Schreurs are with KU Leuven, B-3001 Leuven, Belgium (e-mail: gustavo.avolio@esat.kuleuven.be).

A. Raffo, V. Vadalà, and G. Vannini are with the University of Ferrara, 44122 Ferrara, Italy.

I. Angelov is with Chalmers University of Technology, SE-41296 Gothenburg, Sweden.

G. Crupi and A. Caddemi are with the University of Messina, 98166 Messina, Italy.

Color versions of one or more of the figures in this paper are available online at http://ieeexplore.ieee.org.

Digital Object Identifier 10.1109/TMTT.2014.2359852

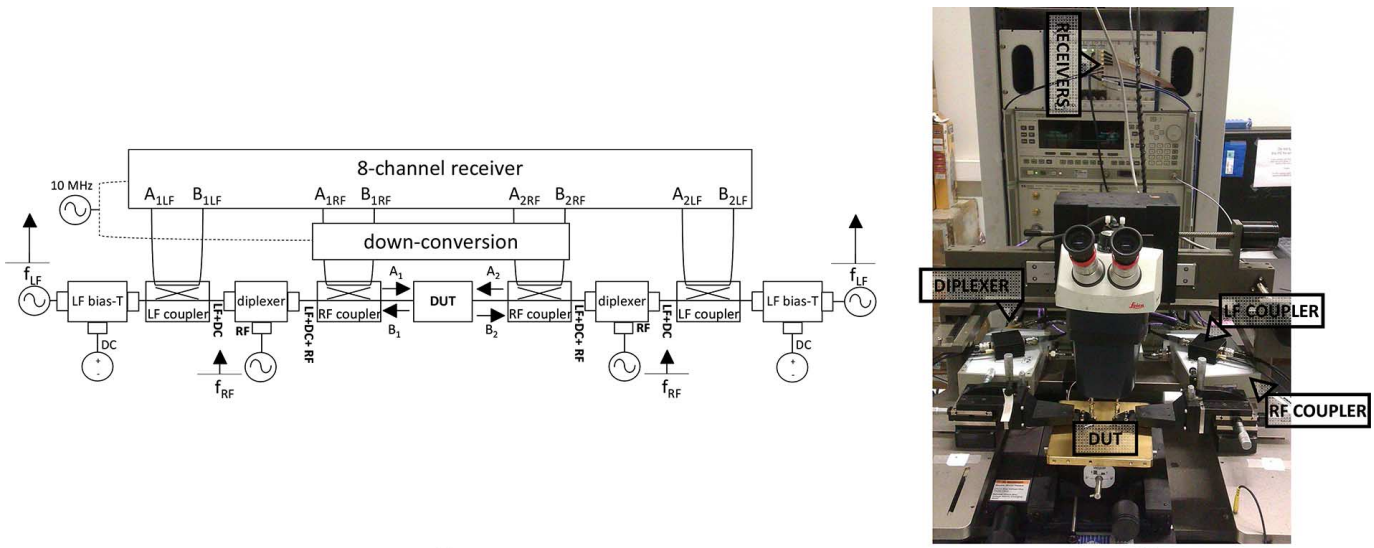

(a) (b)

Fig. 2. Setup for combined LF and RF nonlinear measurements. (a) Block diagram. (b) Photograph.

megahertz range. Along with these low-frequency large signals, a small tickle is applied at RF frequencies. As compared with [17], we have thoroughly extended the theoretical aspects and included many simulation and experimental results in order to assess the validity of the proposed technique. We highlight that, under dynamic-bias operation, one actually does not need to acquire the harmonics of the RF frequency which can be then set as high as the instrument highest value. In addition, another advantage of this approach consists of catching the main transistor nonlinearities by means of a small set of experimental data, thus reducing considerably the measurement time.

The technique that we propose is general and independent of the device technology and operating condition. In this work, we studied a 0.15-μm GaAs pHEMT, designed for resistive mixer applications. In principle, the proposed technique is suitable for use with different analytical model formulations, including [3], [18]–[24].

We used a model available in commercial computer-aided design (CAD) tools [3], which includes self-heating and breakdown. The formulation of the model in [3] is such that an estimate of the main parameters describing the transistor currents and charges can be extracted directly from a small-set of dc and S-parameter measurements and then used as initial values for the optimization against measurements acquired under nonlinear dynamic operation. Moreover, the model in [3] is, by structure, global, and one can target on obtaining a good fit in the operating region of interest. In this work, we focused on resistive mixer operation, and the DUT was biased at $V_{DS} = 0$ V. As the final application was known, we aimed at obtaining a good fit in the triode (linear) region, around the bias-point at $V_{DS} = 0$ V, where self-heating effects or breakdown phenomena are not significant.

In Section III, experimental results along with model extraction are reported. In Section IV, we compare model simulations and experimental data acquired under resistive mixer operation. Conclusions are drawn in the final section.

II. Dynamic-Bias Measurements

A. Dynamic-Bias Concept

The proposed approach is based on the concept of dynamic-bias [17]. Basically, the DUT is driven by large signals at low frequency f_{LF} along with the dc voltages. The dc and the low-frequency signals set the DUT large-signal operating point (LSOP), which includes also the thermal and trapping state of the DUT [7]. On top of the LSOP, a high-frequency tickle at f_{RF} is applied, as shown in Fig. 2.

It is worth noticing that this situation is similar to a small-signal measurement where the LSOP is represented by the dc voltages and the tickle by the ac small signal. Here, the LSOP, which encompasses low-frequency signals, is dynamically varied, as a dynamic-bias, while the tickle is applied on top of it. When only the LSOP is switched on, harmonics of f_{LF} are generated in both the transistor currents and charges. However, the conductive part of the currents (I_G and I_D in Fig. 1) can be straightforwardly measured at low frequencies, whereas the displacement currents associated with the variations of the semiconductor charges (Q_G and Q_D in Fig. 1) can be hardly detected. Instead, when the tickle is switched on, along with the LSOP, the fast variation of the charge induced by the tickle itself around the dynamic LSOP can be detected. Similarly, fast variations will be induced by the tickle in the conductive currents and therefore one can also measure the high-frequency part of it while the LSOP varies dynamically. For explanatory purposes, in Fig. 3, we report the simulations under dynamic-bias condition of a FET model available in a commercial circuit simulator [18].

In Fig. 3(a)–(d), the black line represents the LSOP only. The gray line represents the time-domain waveforms when the tickle is switched on at the input port.

The drain–current time-domain waveform includes both the LSOP and the RF component induced by the tickle. With regard to the gate current, which is mainly capacitive, the component induced by the tickle is much larger than that induced

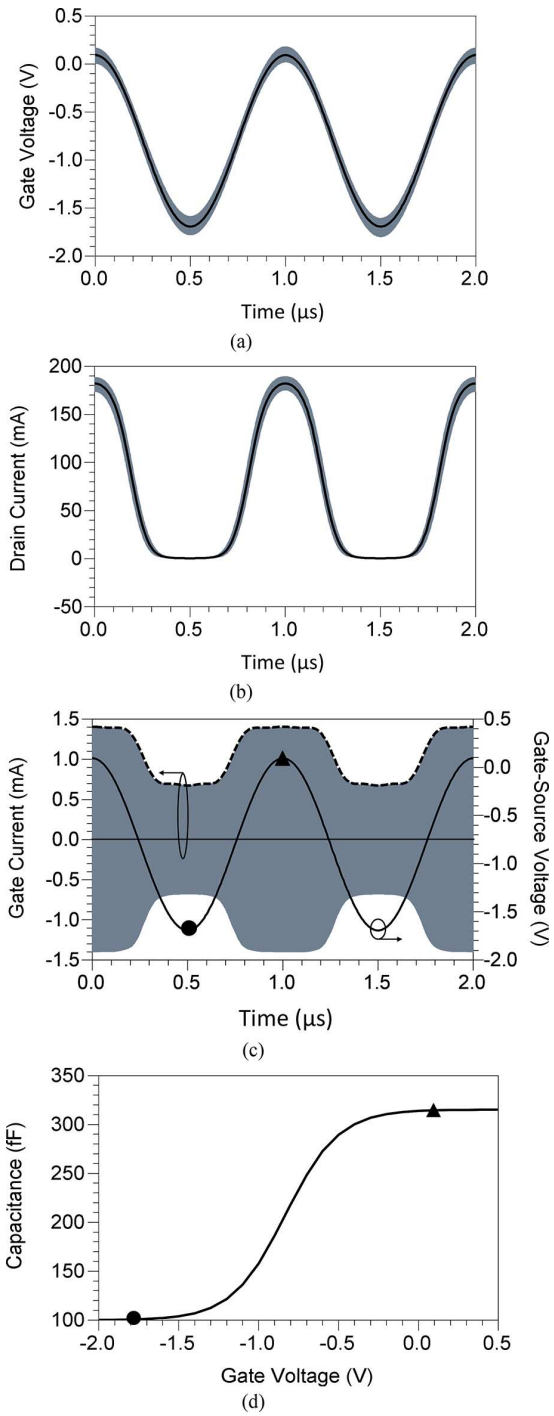

Fig. 3. Simulated response of a CAD available FET nonlinear model under dynamic-bias condition. (a) Gate–voltage time-domain waveform, (b) drain–current time-domain waveform, and (c) gate–current time domain waveform along with the low-frequency gate-voltage waveform. LSOP (black line) and RF + LSOP (gray line). (c) Envelope of the gate–current waveform is also shown (dashed line). (d) Simulated gate capacitance of the chosen FET model is shown. The gate-voltage in (c) sweeps instantaneously from pinch-off region (circle) to open-channel condition (triangle) thus changing dynamically the value of the capacitance which affects the displacement gate current (c). This figure is purely illustrative.

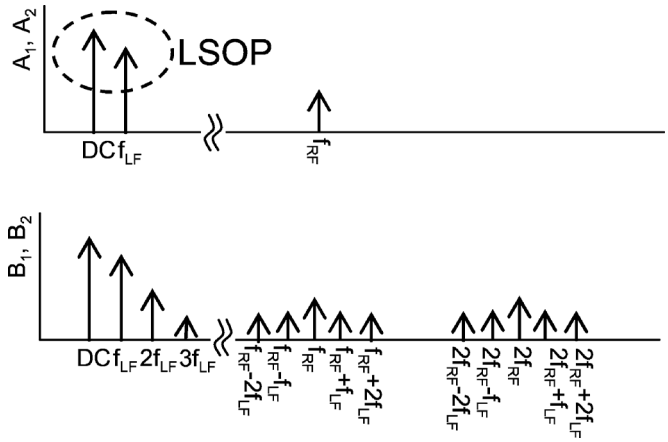

Fig. 4. Frequency spectra of the incident (A_1 and A_2) and scattered (B_1 and B_2) waves under dynamic-bias condition.

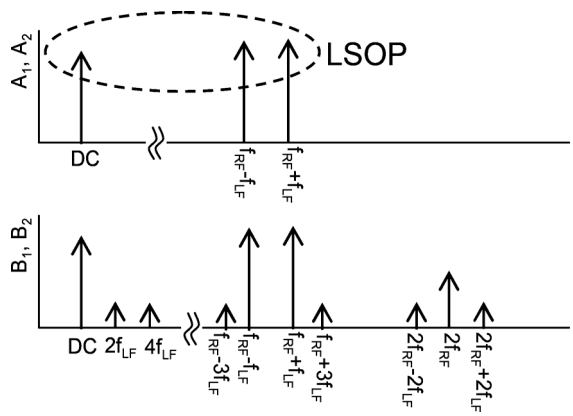

Fig. 5. Frequency spectra of the incident (A_1 and A_2) and scattered (B_1 and B_2) waves under RF two-tone measurements.

by the LSOP. However, in the RF part of the gate current it is clearly observed the effect of the dynamic-bias. The LSOP sinusoidal gate–voltage time-domain waveform, which sweeps from pinch-off to open channel [Fig. 3(a)], dynamically changes the instantaneous value of the gate nonlinear capacitance [Fig. 3(d)] and, as a result, it modulates the amplitude of the displacement current induced by the capacitance itself. In Fig. 3(c), the envelope of the gate–current waveform clearly reflects the nonlinear capacitance behavior. In this example, we have considered the nonlinear gate capacitance. Similar considerations could have been drawn if we had considered a nonlinear resistor or a nonlinear conductive current source.

From the above discussion, a clear advantage of the proposed approach emerges, namely the possibility to span over transistor nonlinearity by means of a single measurement. As compared to multibias dc measurements combined with multibias S-parameters, the dynamic points covered by the LSOP of a single measurement under dynamic-bias condition can be used instead of measurements at several bias-points [25], [26]. By using different LSOPs, one can quickly obtain a full coverage of the input–output voltage plane of interest for the selected application. Additionally, for each LSOP, one can separate the nonlinear dynamic conductive currents, which are contained in the measured LSOP time-domain waveforms, and the nonlinear displacement currents, which are contained in the RF part of the measured time-domain waveforms. This greatly simplifies the

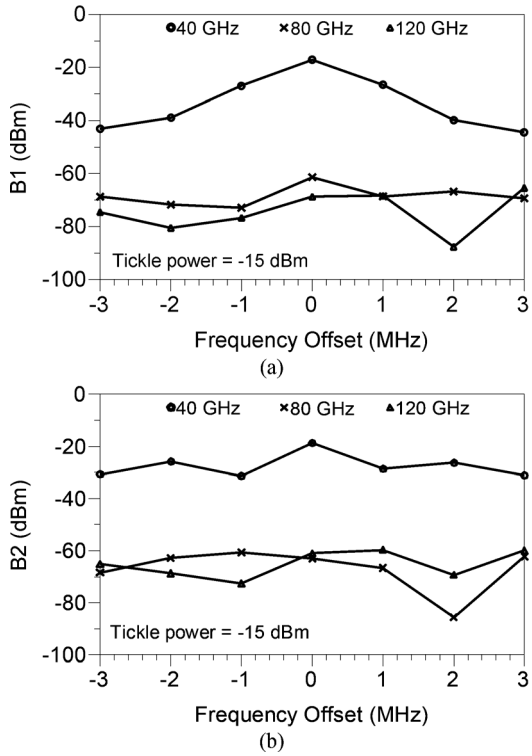

Fig. 6. Simulated scattered waves of a CAD available nonlinear model under dynamic-bias condition at: $\mathrm{V_{GS0}} = -1$ V, $\mathrm{V_{DS0}} = 0$ V, $\mathrm{f_{LF}} = 1$ MHz, and $\mathrm{f_{RF}} = 40$ GHz. Intermodulation products around $\mathrm{f_{RF}}$, $2\mathrm{f_{RF}}$, and $3\mathrm{f_{RF}}$ of (a) $\mathrm{B_1}$ and (b) $\mathrm{B_2}$.

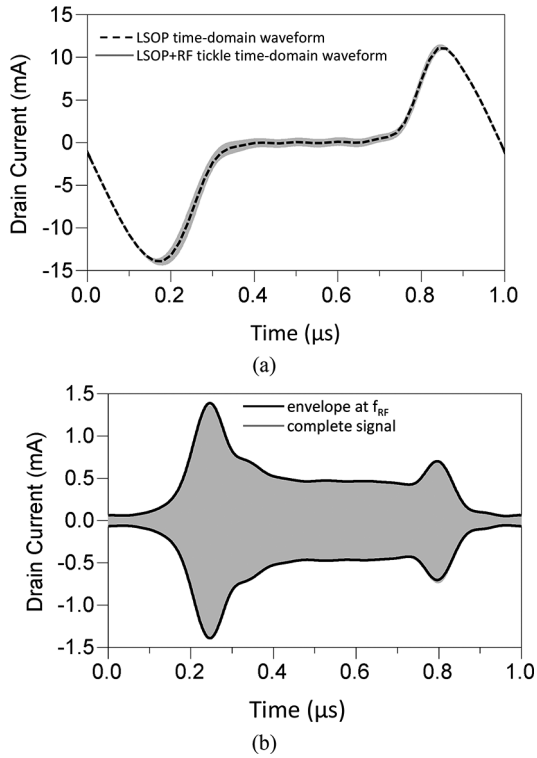

Fig. 7. Simulated response of a CAD available nonlinear model under dynamic-bias condition at: $\mathrm{V_{GS0}} = -1$ V, $\mathrm{V_{DS0}} = 0$ V, $\mathrm{f_{LF}} = 1$ MHz, and $\mathrm{f_{RF}} = 40$ GHz. (a) LSOP time-domain waveform (dashed line) and the $\mathrm{LSOP + RF}$ time-domain waveform (grey line). (b) RF envelope reconstructed from the intermodulation products around $\mathrm{f_{RF}}$ (continuous line) and complete RF signal including response at $\mathrm{f_{RF}}$ harmonics (gray line).

model extraction procedure, since one can split the optimization of the model parameters describing the nonlinear resistive and reactive phenomena.

In Section II-B, a more complete analysis of the dynamic-bias is carried out in the frequency domain. We show that another advantage of such a measurement consists of the ability to set the value of the frequency of the RF tickle even if its harmonics fall beyond the instrument bandwidth.

B. Frequency-Domain Analysis

In the previous section, the proposed approach has been discussed in terms of the dynamic-bias concept and, as a result, the high-frequency current induced by the tickle is actually modulated by the LSOP. This implies in the frequency domain the presence of intermodulation tones [27], [28]. Considering a nonlinear capacitor [27], [28] as follows:

$$\mathrm{C(v)} = \mathrm{C_0} + \mathrm{C_1 v} + \mathrm{C_2 v^2} + \mathrm{C_3 v^3} + \cdots \tag{1}$$

the displacement current i resulting from (1) is

$$\mathrm{i} = \mathrm{C(v)\dot{v}}. \tag{2}$$

Under dynamic-bias condition, the excitation v consists of the dc voltage and ac components at $\mathrm{f_{LF}}$ and $\mathrm{f_{RF}}$.

It is very straightforward to demonstrate [25], [26] that, in periodic steady-state condition, the current as a result of (2) contains frequency components at $\mathrm{nf_{LF}}$ $(\mathrm{n} = 1, \ldots, \mathrm{N})$, at $\mathrm{kf_{RF}}$ $(\mathrm{k} = 1, \ldots, \mathrm{K})$, and $\mathrm{kf_{RF}} \pm \mathrm{nf_{LF}}$.

The spectrum of the incident and scattered waves under dynamic-bias condition is illustrated in Fig. 4. The frequency components at dc and $\mathrm{nf_{LF}}$ represent the LSOP. The intermodulation products around $\mathrm{f_{RF}}$ and its harmonics represent the modulation induced when the tickle is switched on.

As such, the frequency spectra shown in Fig. 4 are not different than those obtained when performing a standard multitone test [28] and shown in Fig. 5 in case of a two-tone measurement. In a standard multi-tone measurement, the LSOP is set directly by the modulated RF carrier frequency. In order to correctly reconstruct the LSOP time-domain waveforms and use them for model extraction, the harmonics of $\mathrm{f_{RF}}$ have to be acquired but they may fall beyond the measurement system bandwidth. With the proposed approach, instead, the LSOP is set by signals applied at low frequencies and several harmonics can be straightforwardly acquired [12]. In addition, if the power of the tickle at $\mathrm{f_{RF}}$ is much lower than the power of the LSOP signals, the harmonics of the tickle can be neglected, along with the intermodulation products around them, without impacting significantly the reconstructed time-domain waveforms. Obviously this is an approximation which should be verified case by case and depending on the operating condition of the DUT. There is not a rigorous way to define how lower the tickle power level should be as compared to the power of the LSOP signals.

In order to verify these assumptions, we performed harmonic-balance simulations by applying large signals at $\mathrm{f_{LF}}$ at both DUT ports and the tickle at $\mathrm{f_{RF}}$ only at the input port while the

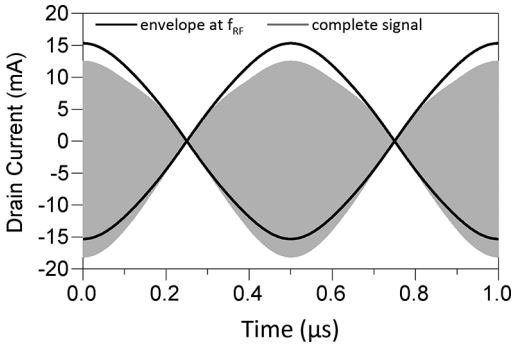

Fig. 8. Simulated RF two-tone response of a CAD available nonlinear model at: $V_{GS0} = -1$ V, $V_{DS0} = 0$ V, $f_{LF} = 1$ MHz, and $f_{RF} = 40$ GHz. RF envelope reconstructed from the intermodulation products around f_{RF} (continuous line) and complete signal including response at f_{RF} harmonics (gray line).

TABLE I
LARGE-SIGNAL OPERATING POINTS

	$A_1(0)$ (V)	$A_1(f_{LF})$ Mag/Phase (V/deg)	$A_2(0)$ (V)	$A_2(f_{LF})$ Mag/Phase (V/deg)
LSOP1	-0.5	0.460/163	0.174	0.474/165
LSOP2	-0.5	0.459/-95	0.142	0.477/-63
LSOP3	-0.5	0.460/12	0.038	0.472/74
LSOP4	-0.5	0.459/7	0.074	0.468/99
LSOP5	-0.5	0.460/-104	0.157	0.469/18
LSOP6	-0.5	0.460/-145	0.204	0.474/8
LSOP7	-0.5	0.461/123	0.218	0.477/-53

output port was terminated with a 50-Ω load. $f_{LF} = 1$ MHz and $f_{RF} = 40$ GHz. The power of the LF signals was 3 dBm, and the power of the tickle was -15 dBm. The device was biased at $V_{GS0} = -1$ V and $V_{DS0} = 0$ V. This situation is very close to our actual experiments and it represents a strongly nonlinear operating condition. In Fig. 6, the simulated input and output scattered waves B_1 and B_2 are reported at $kf_{RF} \pm nf_{LF}$ with $k = (1, 2, 3)$ and $n = (0, 1, 2, 3)$. As it can be observed and for the operating condition set up for the simulation, the intermodulation tones around the second and third harmonic of the tickle are much lower than those around f_{RF}. In Fig. 7 we report the simulated time-domain waveforms reconstructed with and without the harmonics of f_{RF}.

In Fig. 7(a), we report the full time-domain waveform, including the LSOP. In Fig. 7(b), the RF current induced by the tickle (gray line) is plotted without the LSOP contribution and including all the intermodulation products at f_{RF} and its harmonics. In the same figure, we show also the envelope of the time-domain waveform obtained by considering only the intermodulation product around f_{RF}. We did the same for simulated time-domain waveforms obtained with a two-tone excitation, as shown in Fig. 8.

From Fig. 7(b), it emerges that the approximated envelope reconstructed by using only the spectral components around f_{RF} can reproduce well the envelope of the full signal and that the errors introduced by neglecting the harmonics of f_{RF} are not significant. This implies that, as long as the power of the tickle is sufficiently low, the value of f_{RF} can be set as high as the instrument bandwidth.

The situation is different for the two-tone simulation. In this case, the envelope (black line) obtained from only the intermodulation products around f_{RF} differs from the envelope of the full signal, meaning that the harmonics of f_{RF} cannot be ne-

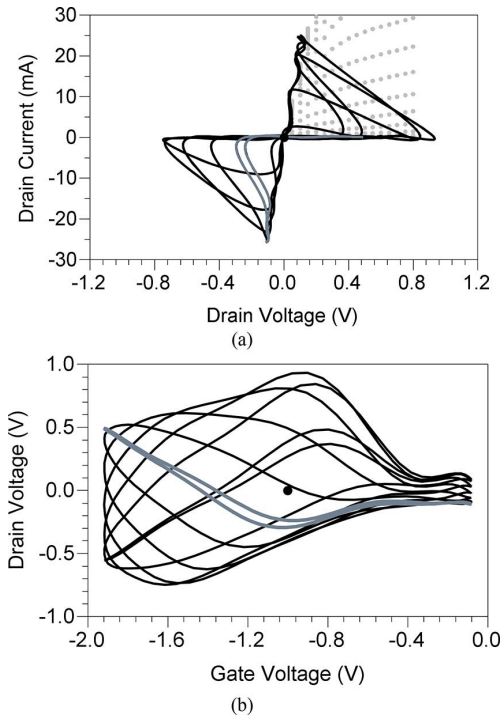

Fig. 9. Measured time-domain trajectories corresponding to the LSOPs in Table I. (a) DC measurements (dots) and measured load lines (lines). (b) Input–output voltage trajectories. The dot represents the bias point. The gray line is the LSOP of the measured spectra around f_{RF} reported in Fig. 10.

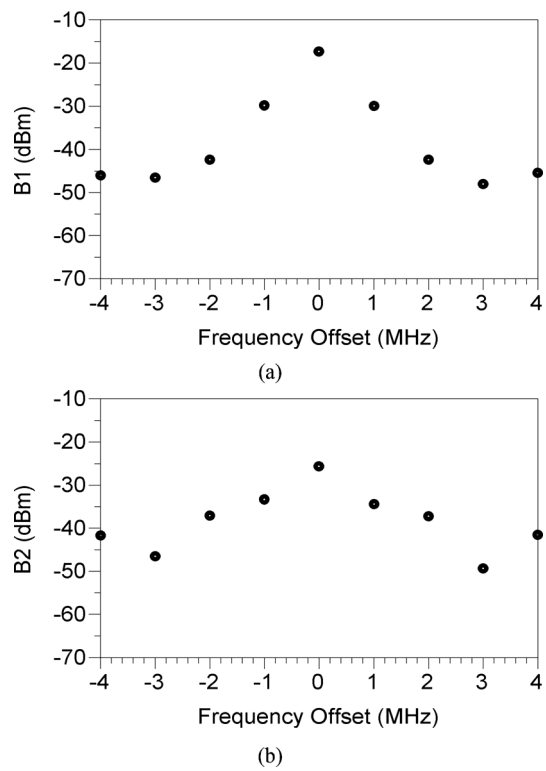

Fig. 10. Measured spectra of the input and output scattered waves around $f_{RF} = 40$ GHz and corresponding to the LSOP highlighted in Fig. 9. $V_{GS0} = -1$V, $V_{DS0} = 0$ V, and $f_{LF} = 1$ MHz.

TABLE II
MODEL PARAMETERS

I_{pk0} (mA)	66	B_1	1.25	R_s (Ω)	0.59	V_j (V)	0.55	C_{gd0} (fF)	40.0
P_1	2.34	B_2	1	L_g (pH)	43.7	I_j (μA)	8.8	P_{10}	2.6
P_2	0	α_R	0.2	L_d (pH)	39.0	P_g	11	P_{11}	3.33
P_3	1.72	α_S	0.86	L_s (pH)	6.8	C_{gsp} (fF)	69.9	P_{20}	0
V_{pks} (V)	-0.28	R_g (Ω)	1.94	C_{pg} (fF)	8.7	C_{gs0} (fF)	37.7	P_{21}	0
DV_{pks} (V)	0.12	R_d (Ω)	0.56	C_{pd} (fF)	8.7	C_{gdp} (fF)	67.0		

glected this time to properly reconstruct the time-domain waveform. This clearly poses a limit to the highest value of f_{RF} as its harmonics must be within the instrument bandwidth.

In Section III, we apply dynamic-bias measurements to a transistor designed for resistive-mixer operation. The acquired measurements are then used for the extraction of a nonlinear model whose equations are available in the circuit simulator [18].

III. Experimental Results and Model Extraction

A. Measurements

We performed dynamic-bias measurements on a 0.15×300 μm^2 GaAs pHEMT. Experimental data were acquired with a 50-GHz LSNA extended at low frequencies [13] and with eight vector-calibrated acquisition channels (see Fig. 2). Four channels were used to acquire the LSOPs, and the other four channels were used to acquire the intermodulation tones around f_{RF}, which was set equal to 40 GHz. The power of the tickle, applied only at the input port, was set equal to -15 dBm. The device was biased at $V_{GS0} = -1$ V and $V_{DS0} = 0$ V. In Table I, the phasors of the incident waves used to set the acquired LSOPs are reported. The LSOPs in Table I correspond to the measured dynamic trajectories shown in Fig. 9. Clearly, as a result of few measurements (seven in total in this case), one can straightforwardly cover a wide range of input and output voltages, thus exciting the DUT nonlinearities in all the operating regions of interest, including instantaneous negative values of the drain–source voltage. Differently from applying LSOPs at higher frequencies, at low frequencies one can get the transistor conductive currents directly from the one induced at the LSOPs as these are not mixed with the displacement currents. If the frequency of the LSOPs is higher than the cut-off frequency of dispersive phenomena linked to the presence of traps in the semiconductor materials, it is reasonable to assume that the conductive current is frequency independent. Although this assumption depends on the DUT technology, experimental results reported in literature [7], [12] suggest that it is valid for III–V semiconductors in the megahertz range. Also, separating the conductive currents from the displacement ones is advantageous within the model extraction phase.

For each LSOP in Table I, a tickle at f_{RF} was applied at the input port. As a result, intermodulation tones are induced around f_{RF}, and they are acquired synchronously with the LSOPs frequency spectra by an eight-channel LSNA. In Fig. 10, we report the measured intermodulation tones corresponding to the LSOP highlighted with gray thick line in Fig. 9.

The LF and RF spectra corresponding to the LSOPs in Table I are used to optimize the model parameters as described in Section II-B. In this work, we use the Chalmers model formulation [3], [18] whose parameters describing the conductive currents can be directly linked to the shape of the current time-domain waveform or to its spectral components and therefore their value can be adjusted accordingly.

B. Model Extraction

The parameters of the model [3] are obtained by numerical optimization against the measurements shown in the previous section. Before running numerical optimization, we estimated the initial values of the parameters of the FET model as follows [28]–[30] (see the Appendix):

1) estimation of the initial values of the parasitic elements (C_{pg}, R_g, L_g, R_s, L_s, R_d, L_d, and C_{pd});
2) estimation of the initial values of the parameters of the resistive gate current;
3) estimation of the initial values of the main parameters of the resistive drain current I_D;
4) estimation of the initial values of the main parameters of the capacitance model.

To accomplish 1) and 4), we performed a few multibias S-parameter measurements. Specifically, for the initial estimation of the parasitic element values, we used S-parameters measured at $V_{DS} = 0$ V [26], [31]. For the initial values of the capacitances, we used the imaginary part of the Y-parameters obtained from measured S-parameters at $V_{DS} = 0$ V and few V_{GS} values from pinch-off to open channel in order to obtain directly from measured data the initial values for C_{gsp}, C_{gdp}, C_{gs0}, C_{gd0}, P_{10}, P_{11}, P_{40}, and P_{41}.

With regard to the parameters of the current I_G and I_D, initial values were obtained from dc measurements performed by sweeping V_{GS} at $V_{DS} = 0$ V, $V_{DS} = 0.2$ V, and $V_{DS} > V_{knee}$. In this way, one can obtain the I_G model parameters I_j, V_j, and P_G and the main I_D model parameters: I_{pk0}, V_{pks}, D_{vpks}, and P_1. In some cases, good initial estimates of some of the parameters may be inferred from data provided by the foundry.

Next, we performed numerical optimization. We defined the optimization goals as the difference, at each point of the full frequency grid of the measurements, between the real and imaginary parts of the measured and simulated input and output scattered waves. First, we ran optimization with a random-based search algorithm. We refined the parameters values by running a gradient-based algorithm.

The parameter vector of the equation describing the conductive drain current (I_D in Fig. 1) was optimized against the low-frequency part of the spectra of the measurements in Table I. The parameters of the capacitive part of the model (Q_G and Q_D in Fig. 1) and the linear parasitic elements (C_{pg}, R_g, L_g, R_s, L_s, R_d, L_d, and C_{pd} in Fig. 1) were optimized against the measured

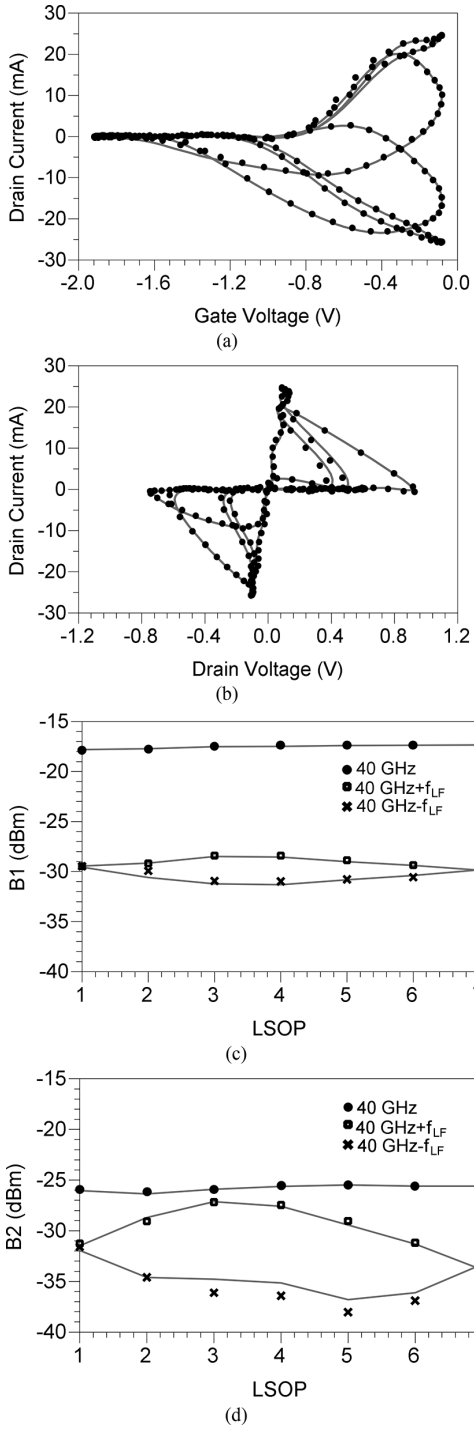

Fig. 11. Measurements (symbols) and simulations of the extracted model (lines) at $V_{GS0} = -1$ V, $V_{DS0} = 0$ V, $f_{LF} = 1$ MHz, and $f_{RF} = 40$ GHz. (a) Dynamic transcharacteristics, (b) dynamic load lines, (c) B1 at f_{RF} and $f_{RF} \pm f_{LF}$, and (d) B2 at f_{RF} and $f_{RF} \pm f_{LF}$.

intermodulation tones appearing in the spectra of the measurements in Table I. The values of the model parameters obtained after optimization are reported in Table II. The measured and simulated LSOPs are reported in Fig. 11(a) and (b). The measured and simulated intermodulation tones around f_{RF} for each LSOP are illustrated in Fig. 11(c) and (d), and, in both cases, the agreement is good.

In Fig. 12, we report the comparison between experimental data and model simulations performed by sweeping the input

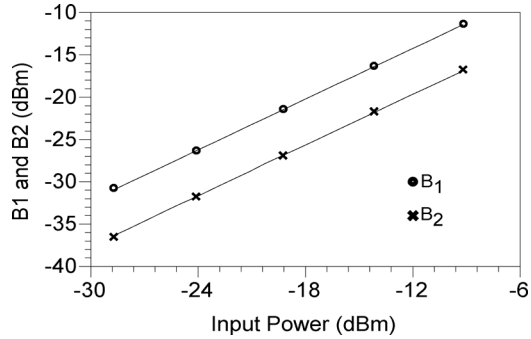

Fig. 12. Measurements (symbols) and simulations of the extracted model (lines) at $V_{GS0} = -1$ V, $V_{DS0} = 0$ V, $f_{RF} = 40$ GHz, and swept input power.

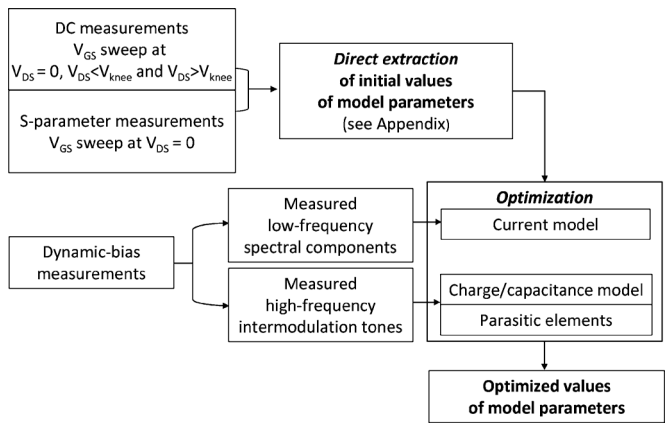

Fig. 13. Block diagram of the model extraction procedure.

power at 40 GHz. The good agreement at low power levels confirms that the model yields good prediction capability also under small-signal operation.

The block diagram of the extraction procedure is shown in Fig. 13.

IV. Resistive Cold-FET Mixer Measurements

Measurements to validate the model have been performed with an LSNA [32]. The device was biased for resistive-mixer operation [33], and signals were injected at the input and output port in order to mimic the mixer-like behavior. A large-signal was applied at the input port, acting as the local oscillator (LO), at frequencies (f_{LO}) between 31.25 GHz and 40 GHz. A small-signal was applied at the output port at $f_{IF} = 2.5$ GHz. The power of the LO signal was equal to 9.7 dBm and the power of the IF signal was equal to -13.5 dBm.

In Fig. 14, we report the magnitude of the waves B_1 and B_2 acquired by the LSNA at f_{LO} and $f_{LO} \pm f_{IF}$ as function of the LO frequency. In Fig. 15, a snapshot of the measured and simulated drain current and voltage time-domain waveforms at $f_{LO} = 35$ GHz is reported. The power of the input signal at f_{LO} is equal to 9.7 dBm and the power of the input signal at f_{IF} is equal to -13.5 dBm. Finally, we show the comparison between the measurements and simulations of the upper conversion gain as the ratio between the power at $f_{LO} + f_{IF}$ and the power at f_{IF}. Results are shown in Fig. 16 at different power levels of the LO signal and three values of the output impedance at $f_{LO} + f_{IF}$, which was varied with a manual tuner. The obtained agreement between the simulated and measured conversion gain is good. In

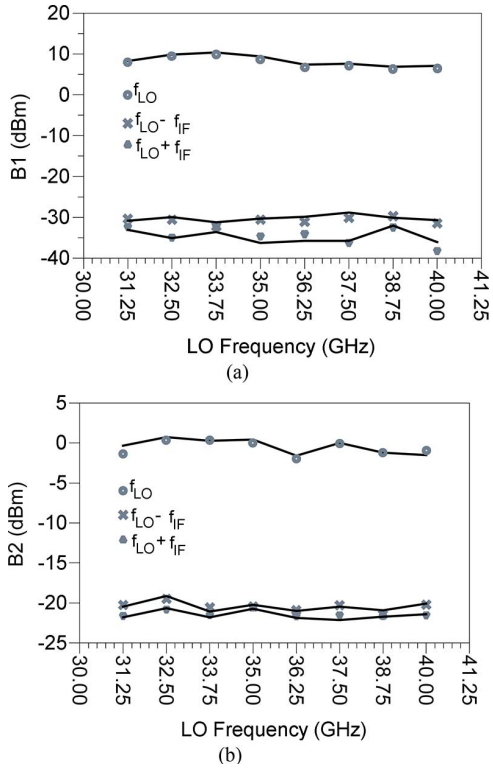

Fig. 14. Measurements (gray symbols) and simulations (line) of the extracted model at $V_{GS0} = -1$ V, $V_{DS0} = 0$ V, and $f_{IF} = 2.5$ GHz as function of the LO frequency.

the inset of Fig. 17, the good agreement between measurements and simulation is highlighted for the highest values of power.

V. Conclusion

We extracted the nonlinear model of a transistor for resistive mixer operation. The extraction is performed starting from measurements performed under dynamic-bias condition. This approach is advantageous as compared to standard multibias dc and S-parameter measurements in terms of amount of experimental data to collect and measurement time.

The DUT is driven into the nonlinear regime by signals applied at low frequencies while a small-signal is applied at RF frequencies. As compared with standard RF nonlinear measurements, the main nonlinearities of the tested devices are driven by low-frequency signals, thus overcoming the limitation of today's RF measurement systems bandwidth. In addition, as a result of dynamic-bias measurements, one can separate the nonlinear dynamic conductive currents from the nonlinear displacement currents induced by the RF tickle. This represents a clear advantage within the model extraction phase.

Appendix
Extraction of Initial Values of Model Parameters

Here, we describe the steps to obtain initial values of some model parameters. More details on the complete extraction procedure can be found in [30].

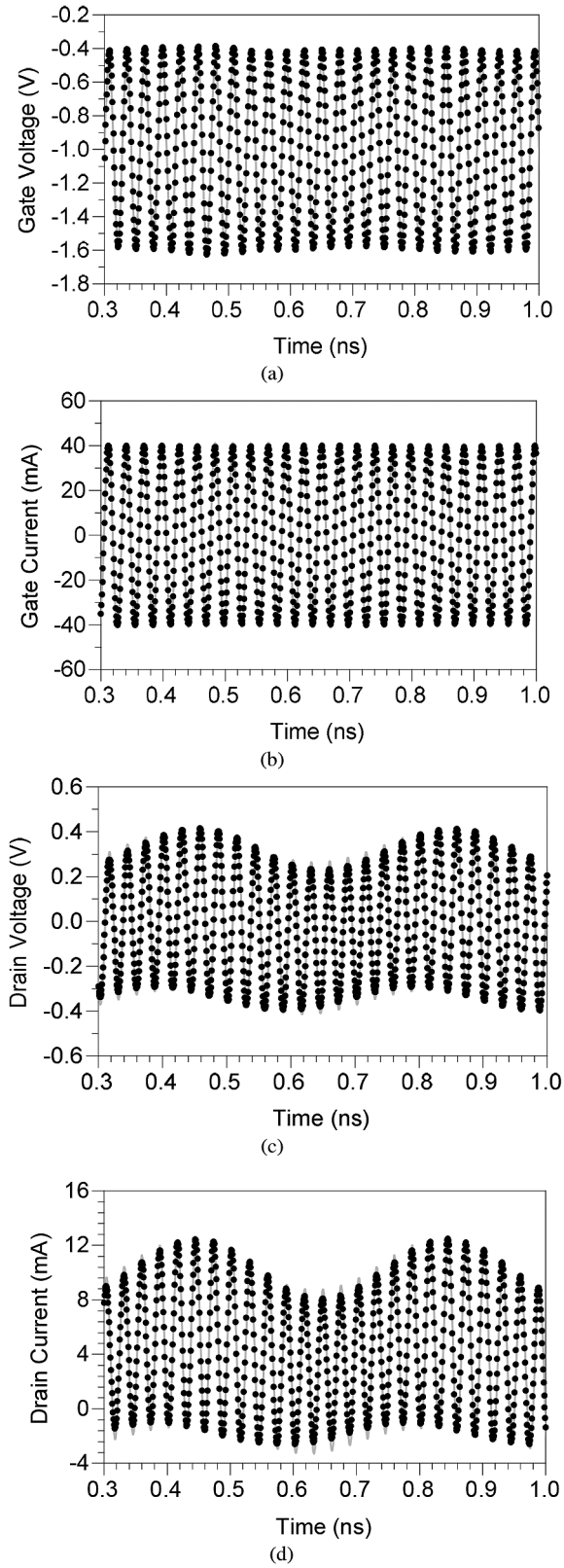

Fig. 15. Snapshot of the measured (symbols) and simulated (line) time-domain waveforms considering the spectral components around f_{LO}: (a) gate voltage, (b) gate current, (c) drain voltage, and (d) drain current at $f_{LO} = 35$ GHz, $f_{IF} = 2.5$ GHz, $P_{LO} = 9.7$ dBm, $P_{IF} = -13.5$ dBm, $V_{GS0} = -1$ V, and $V_{DS0} = 0$ V.

The first step consists of determining the parasitic elements. In this work and for the considered DUT, we used well-known

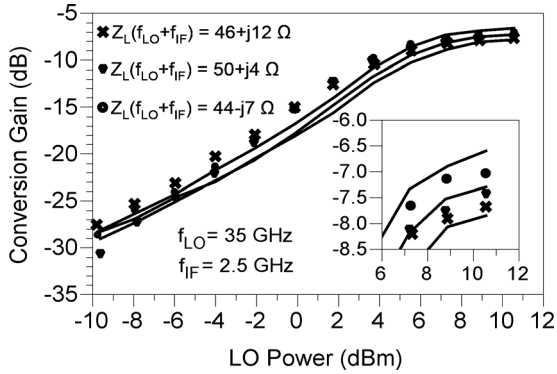

Fig. 16. Measured (symbols) and simulated (lines) conversion gain as function of the LO power at: $f_{LO} = 35$ GHz, $f_{IF} =$ GHz, $P_{IF} = -13.5$ dBm, $V_{GS0} = -1$ V, $V_{DS0} = 0$ V, and $Z_L(f_{LO}+f_{IF})$ equal to $46+j12\ \Omega$ (crosses), $50+j4\ \Omega$ (triangles), and $44-j7\ \Omega$ (circles).

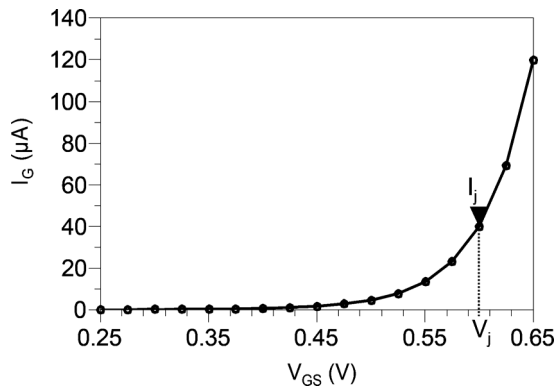

Fig. 17. Measured dc $I_G - V_{GS}$ at $V_{DS} = 0$ V.

existing techniques [26], [31]. In the following, we explain how to extract the initial values for the resistive currents and the charge or capacitance model.

A. I_G Model

The equation for the current I_G is [18]

$$I_G = I_j * \left(e^{P_G*(\tanh(2*(V_{GS}-V_j)))} - e^{P_G*(\tanh(-2*V_j))} \right). \tag{3}$$

Initial values of I_j, P_G, and V_j can be obtained from measured dc $I_G - V_{GS}$ at $V_{DS} = 0$ V, as shown in Fig. 17.

V_j is the Schottky junction built-in voltage and P_G is a parameter from which the junction ideality factor is computed.

From (3), $I_G \sim I_j$ at $V_{GS} = V_j$. Also, the derivative of (3) as a function of V_{GS} is equal to $2 * I_j * P_G$ when $V_{GS} = V_j$. From the numerical derivative of the data in Fig. 17, P_G can be calculated. In many cases, the default value of P_G set in the circuit simulator can be used.

B. Capacitance Model

The equations of the capacitances model (C_{gs} and C_{gd}), at $V_{DS} = 0$V, are the following [18]:

$$C_{gs} = C_{gsp} + C_{gs0} * (1 + \tanh(P_{10} + P_{11} * V_{GS})) * (1 + \tanh(P_{20})) \tag{4}$$

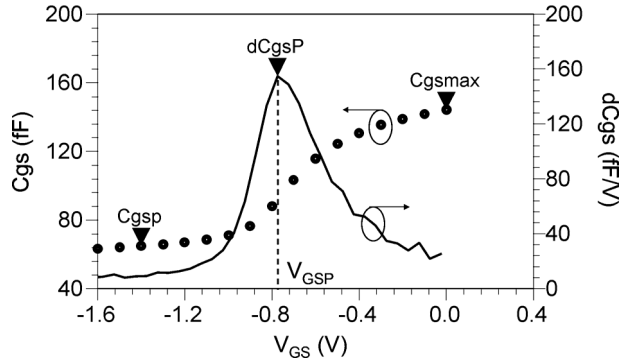

Fig. 18. C_{gs} derived from multibias S-parameter measurements (dots) and its derivative versus V_{GS} (line). $V_{DS} = 0$ V.

$$C_{gd} = C_{gdp} + C_{gd0} * (1 + \tanh(P_{40} + P_{41} * V_{GS})) * (1 + \tanh(P_{30})). \tag{5}$$

For the initial estimation, we set $P_{20} = P_{30} = 0$. C_{gs}, and C_{gd} as functions of V_{GS} can be obtained from the measured multibias Y-parameters, after de-embedding the parasitic elements. As widely known

$$C_{gs} = \mathrm{Im}(Y_{11} + Y_{12})/\omega \text{ and } C_{gd} = -\mathrm{Im}(Y_{12})/\omega \tag{6}$$

where $\omega = 2\pi f$ and f is the frequency.

From the data plotted in Fig. 18, one can obtain directly the value of C_{gsp}. Also, at high values of V_{GS}, we have

$$C_{gs} = C_{gsmax} = C_{gsp} + 2 * C_{gs0} \tag{7}$$

from which C_{gs0} can be calculated. In the same figure we report the derivative of the C_{gs} versus V_{GS}. From (4) and assuming $P_{20} = 0$, the peak occurs when

$$P_{10} + P_{11} * V_{GSP} = 0 \tag{8}$$

$$dC_{gsP} = P_{11} * C_{gs0} \tag{9}$$

from which P_{10} and P_{11} can be calculated. Same calculations can be done for the parameters in (5). Note that for a device with symmetric geometry with respect to the gate contact, $P_{11} = P_{41}$ and $P_{10} = P_{40}$.

C. I_D Model

The equation of the I_D current is [18]

$$I_D = I_{pk0} * (1 + \tanh(\varphi)) * \tanh(\alpha * V_{DS}) * (1 + \lambda * V_{DS}) \tag{10}$$

with

$$\varphi = P_1 * (V_{GS} - V_{pks}) + P_2 * (V_{GS} - V_{pks})^2 + P_3 * (V_{GS} - V_{pks})^3. \tag{11}$$

For α, we used the default values which are set in the CAD simulator. Otherwise, the extraction can be performed as explained in [30]. Initial values of P_1, V_{pks}, I_{pk0}, and λ can be

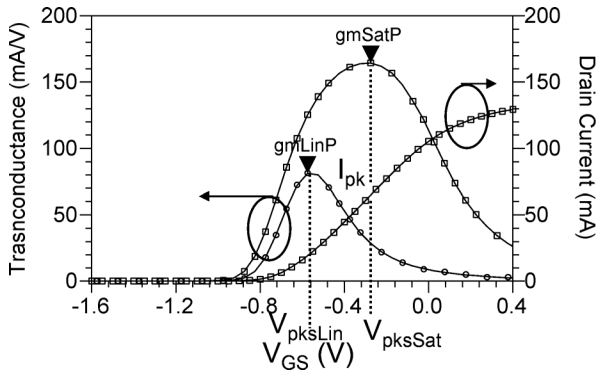

Fig. 19. Measured dc $I_D - V_{GS}$ and transconductance at $V_{DS} > V_{knee}$ (squares) and measured transconductance at $V_{DS} = 0.2$ V (circles).

directly calculated from dc I–V measurements in saturation region $(V_{DS} > V_{knee})$. λ can be derived from the slope of the dc $I_D - V_{DS}$ in saturation region and, although its effect is negligible in linear region, it is needed to calculate the initial value of I_{pk0}. The latter can be derived from the measured dc $I_D - V_{GS}$ at $V_{DS} > V_{knee}$ and the transconductance, as shown in Fig. 19.

In saturation, at $V_{GS} = V_{pksSat}$, we have

$$g_{mSatP} = P_1 * I_{pk} \tag{12}$$

and

$$I_{pk} = I_{pk0} * (1 + \lambda * V_{DS}) \tag{13}$$

from which I_{pk0} can be calculated.

At $V_{GS} = V_{pksSat}$ also P_2 and P_3 can be calculated from the second and third order derivative of the measured current. Practically, it is sufficient, for initial estimation, to calculate P_1 and then set P_2 and P_3 equal to 0 and then optimize them.

In Fig. 19 we show also the measured transconductance at $V_{DS} = 0.2$ V (linear region) from which V_{pksLin} can be obtained and used to calculate the shift (DV_{pks}) with respect to V_{pksSat}.

REFERENCES

[1] D. Schreurs, J. Verspecht, B. Nauwelaers, A. Van de Capelle, and M. Van Rossum, "Direct extraction of the non-linear model for two-port devices from vectorial non-linear network analyzer measurements," in *Proc. Eur. Microw. Conf.*, Sep. 1997, pp. 921–926.

[2] M. C. Curras-Francos, P. J. Tasker, M. Fernandez-Barciela, S. S. O'Keefe, Y. Campos-Roca, and E. Sanchez, "Direct extraction of nonlinear FET I-V functions from time domain large signal measurements," *Electron. Lett.*, vol. 34, no. 21, pp. 1993–1994, Oct. 1998.

[3] I. Angelov, N. Rorsman, J. Stenarson, M. Garcia, and H. Zirath, "An empirical table-based FET model," *IEEE Trans. Microw. Theory Techn.*, vol. 47, no. 12, pp. 2350–2357, Dec. 1999.

[4] M. C. Curras-Francos, P. J. Tasker, M. Fernandez-Barciela, Y. Campos-Roca, and E. Sanchez, "Direct extraction of nonlinear FET Q-V functions from time domain large signal measurements," *IEEE Microw. Guided Wave Lett.*, vol. 10, no. 12, pp. 531–533, Dec. 2000.

[5] J. J. Xu, D. Gunyan, M. Iwamoto, A. Cognata, and D. E. Root, "Measurement-based non-quasi-static large-signal FET model using artificial neural networks," in *IEEE MTT-S Int. Microw. Symp. Dig.*, Jun. 2006, pp. 469–472.

[6] G. Crupi, D. M. M.-P. Schreurs, D. Xiao, A. Caddemi, B. Parvais, A. Mercha, and S. Decoutere, "Determination and validation of new nonlinear FinFET model based on lookup tables," *IEEE Microw. Wireless Compon. Lett.*, vol. 17, no. 5, pp. 361–363, May 2007.

[7] A. Raffo, G. Bosi, V. Vadalà, and G. Vannini, "Behavioral modeling of GaN FETs: A load-line approach," *IEEE Trans. Microw. Theory Techn.*, vol. 62, no. 1, pp. 73–82, Jan. 2014.

[8] J. J. Xu, J. Horn, M. Iwamoto, and D. E. Root, "Large-signal FET model with multiple time scale dynamics from nonlinear vector network analyzer data," in *IEEE MTT-S Int. Microw. Symp. Dig.*, May 2010, pp. 417–420.

[9] J. Verspecht, "Calibration of a measurement system for high frequency nonlinear devices," Ph.D. dissertation, Dept. ELEC, Vrije Universiteit Brussel, Brussel, Belgium, 1995.

[10] Y. Rolain, W. Van Moer, G. Vandersteen, and J. Schoukens, "Why are nonlinear microwave systems measurements so involved," *IEEE Trans. Instrum. Meas.*, vol. 53, no. 3, pp. 726–729, Jun. 2004.

[11] P. S. Blockley, D. Gunyan, and J. B. Scott, "Mixer-based, vector-corrected, vector signal/network analyzer offering 300 kHz–20 GHz," in *IEEE MTT-S Int. Microw. Symp. Dig.*, Jun. 2005, pp. 1497–1500.

[12] A. Raffo, S. di Falco, V. Vadalà, and G. Vannini, "Characterization of GaN HEMT low-frequency dispersion through a multiharmonic measurement system," *IEEE Trans. Microw. Theory Techn.*, vol. 58, no. 9, pp. 2490–2496, Sep. 2010.

[13] G. Pailloncy, G. Avolio, M. Myslinski, Y. Rolain, M. Vanden Bossche, and D. Schreurs, "Large-signal network analysis including baseband," *IEEE Microw. Mag.*, vol. 12, no. 2, pp. 77–86, Mar. 2011.

[14] J. Verspecht and D. E. Root, "Poly harmonic distortion modeling," *IEEE Microw. Mag.*, vol. 7, no. 3, pp. 44–57, Jun. 2006.

[15] H. Qi, J. Benedikt, and P. J. Tasker, "Nonlinear data utilization: From direct data lookup to behavioral modeling," *IEEE Trans. Microw. Theory Techn.*, vol. 57, no. 6, pp. 1425–1432, Jun. 2009.

[16] J. Cai, J. King, B. Merrick, and T. Brazil, "Padé-approximation-based behavioral modeling," *IEEE Trans. Microw. Theory Techn.*, vol. 61, no. 12, pp. 4418–4427, Dec. 2013.

[17] G. Avolio, A. Raffo, I. Angelov, V. Vadalà, G. Crupi, A. Caddemi, G. Vannini, and D. Schreurs, "Nonlinear model for 40 GHz cold-FET operation," in *Proc. IEEE Int. Workshop Integr. Nonlinear Microw. Millimetre-Wave Circuits*, Apr. 2014, pp. 1–3.

[18] Nonlinear Devices. Agilent ADS, Palo Alto, CA, USA, 2003.

[19] W. R. Curtice, "A MESFET model for use in the design of GaAs integrated circuits," *IEEE Trans. Microw. Theory Techn.*, vol. MTT-28, pp. 448–455, May 1980.

[20] A. Materka and T. Kacprzak, "Computer calculation of large-signal GaAs FET amplifier characteristics," *IEEE Trans. Microw. Theory Techn.*, vol. MTT-33, pp. 129–135, Feb. 1985.

[21] H. Statz, P. Newman, I. Smith, R. Pucel, and H. Haus, "GaAs FET device and circuits simulation in SPICE," *IEEE Trans. Electron Devices*, vol. ED-34, no. 2, pp. 160–169, Feb. 1987.

[22] V. I. Cojocaru and T. Brazil, "A scalable general-purpose model for microwave FET's including DC/AC dispersion effects," *IEEE Trans. Microw. Theory Techn.*, vol. 45, pp. 2248–2255, Dec. 1997.

[23] C. Fager, J. C. Pedro, N. B. de Carvalho, and H. Zirath, "Prediction of IMD in LDMOS transistor amplifiers using a new large-signal model," *IEEE Trans. Microw. Theory Techn.*, vol. 50, no. 12, pp. 2834–2842, Dec. 2002.

[24] P. M. Cabral, J. C. Pedro, and N. B. Carvalho, "Nonlinear device model of microwave power GaN HEMTs for high power-amplifier design," *IEEE Trans. Microw. Theory Techn.*, vol. 52, no. 11, pp. 2585–2592, Nov. 2004.

[25] V. Di Giacomo, A. Santarelli, A. Raffo, P. A. Traverso, D. Schreurs, J. Lonac, D. Resca, G. Vannini, F. Filicori, and M. Pagani, "Accurate nonlinear electron device modeling for cold FET mixer design," in *Proc. Eur. Microw. Integr. Circuits Conf.*, Oct. 2008, pp. 294–297.

[26] G. Crupi, A. Raffo, G. Sivverini, G. Bosi, G. Avolio, D. Schreurs, A. Caddemi, and G. Vannini, "Non-linear look-up table modeling of GaAs HEMTs for mixer application," in *Proc. IEEE Int. Workshop Integrated Nonlinear Microw. Millimetre-Wave Circuits*, Sep. 2012, pp. 1–3.

[27] S. A. Maas, *Nonlinear Microwave and RF Circuits*. Norwood, MA, USA: Artech House, 2003.

[28] J. C. Pedro and N. B. Carvalho, *Intermodulation Distortion in Microwave and Wireless Circuits*. Norwood, MA, USA: Artech House, 2003.

[29] I. Angelov, M. Ferndahl, M. Gavell, G. Avolio, and D. Schreurs, "Experiment design for quick statistical FET large signal model extraction," in *Proc. Automatic RF Techn. Group Conf.*, Jun. 2013, pp. 1–5.

[30] I. Angelov, G. Avolio, and D. Schreurs, "Large-signal time-domain waveform-based transistor modeling," in *Microwave De-Embedding: From Theory to Application*, G. Crupi and D. M. M.-P. Schreurs, Eds. Oxford, U.K.: Academic, 2013, ch. 5.

[31] G. Dambrine, A. Cappy, F. Heliodore, and E. Playez, "A new method for determining the FET small-signal equivalent circuit," *IEEE Trans. Microw. Theory Techn.*, vol. 36, no. 7, pp. 1151–1159, Jul. 1988.

[32] D. Schreurs, J. Verspecht, B. Nauwelaers, A. Barel, and M. van Rossum, "Waveform measurements on a HEMT resistive mixer," in *Proc. Automatic RF Techn. Group Conf.*, San Francisco, CA, USA, June 1996, vol. 29, pp. 129–135.
[33] S. A. Maas, *Microwave Mixers*. Norwood, MA, USA: Artech House, 1993.

Gustavo Avolio (M'12) was born in Cosenza, Italy, in 1982. He received the M.Sc. degree in electronic engineering from the University of Calabria, Calabria, Italy, in 2006. and the Ph.D. degree in electronic engineering from KU Leuven, Leuven, Belgium, in 2012.

He is currently a Postdoctoral Researcher supported by FWO Vlaanderen (Belgium). Several times he has been a Visiting Scientist with the University of Ferrara, Ferrara, Italy. In 2013, he was a Visiting Scientist with the National Institute of Standards and Technology (NIST), Boulder, CO, USA. His research work focuses on large-signal measurements and nonlinear modeling of advanced microwave devices.

Antonio Raffo (S'04–M'07) was born in Taranto, Italy, in 1976. He received the M.S. degree in electronic engineering (with honors) and Ph.D. degree in information engineering from the University of Ferrara, Ferrara, Italy, in 2002 and 2006, respectively.

Since 2002, he has been with the Engineering Department, University of Ferrara, Ferrara, Italy, where he is currently a Research Associate and teaches courses in semiconductor devices and electronic instrumentation and measurement. His research activities are mainly oriented to nonlinear electron device characterization and modeling and circuit-design techniques for nonlinear microwave and millimeter-wave applications. He has coauthored over 100 publications in international journals and conferences.

Dr. Raffo is a member of the IEEE Microwave Theory and Techniques Society (MTT-S) MTT-11 Technical Committee. He served as Technical Program Chair for the IEEE International Workshop on Integrated Nonlinear Microwave and Millimetre-wave Circuits (INMMiC), Leuven, Belgium, 2014.

Iltcho Angelov was born in Bulgaria. He received the M.Sc. degree in electronics (with honors) and Ph.D. degree in physics and mathematics from Moscow State University, Moscow, Russia.

From 1969 to 1991, he was with Institute of Electronics, Bulgarian Academy of Sciences, Sofia, Bulgaria, as a Researcher, Research Professor, and Head of the Department of Microwave Solid State Devices (1982). Since 1992, he has been with Chalmers University, Göteborg, Sweden, as a Research Professor. As a Researcher, he has worked with various microwave devices, including Impatt, Gunn, bipolar junction transistors, field-effect transistors (FETs), low-noise and low-power amplifiers, oscillators, synchronization and phase modulation, frequency dividers, multipliers, and low-noise receivers up to 220 GHz. In recent years his main activity is related to FET and HBT modeling. Together with CAD companies FET GaAs, and later GaN high-electron mobility transistor model was implemented in various CAD tools.

Valeria Vadalà (S'07–M'11) was born in Reggio Calabria, Italy, in 1982. She received the M.S. degree (with honors) in electronic engineering from the "Mediterranea" University of Reggio Calabria, Reggio Calabria, Italy, in 2006, and the Ph.D. degree in information engineering from the University of Ferrara, Ferrara, Italy, in 2010.

She is currently with the Department of Engineering, University of Ferrara, Ferrara, Italy. Her research interests include nonlinear electron-device characterization and modeling and circuit-design techniques for nonlinear microwave and millimeter-wave applications.

Giovanni Crupi (S'04–M'12–SM'13) was born in Lamezia Terme, Italy, in 1978. He received the M.Sc. degree in electronic engineering (*cum laude*) and Ph.D. degree from the University of Messina, Messina, Italy, in 2003 and 2006, respectively.

Currently, he is an Assistant Professor with the University of Messina, Messina, Italy, where he has taught courses on microwave electronics, optoelectronics, and bioengineering. Since 2005, he has been a repeat Visiting Scientist with the University of Leuven (KU Leuven), Leuven, Belgium, and the Interuniversity Microelectronics Center (IMEC), Leuven. He has authored or coauthored over 100 publications in international journals and conferences and two book chapters. He has coedited the book *Microwave De-embedding: From Theory To Applications* (Academic, 2013). His main research interests include small- and large-signal modeling of advanced microwave devices.

Dr. Crupi is the Chair of the IEEE Microwave Theory and Techniques Society (MTT-S) Fellowship program. He serves as an associate editor of the *International Journal of Numerical Modelling: Electronic Networks, Devices and Fields*. He also serves as Technical Program Committee Chair for the IEEE International Workshop on Integrated Nonlinear Microwave and Millimetre-wave Circuits (INMMiC), Taormina, Italy, 2015.

Alina Caddemi (M'13) received the degree in electronic engineering (with honors) and Ph.D. degree from the University of Palermo, Palermo, Italy, in 1982 and 1987, respectively.

In 1984, she joined the Electrical Engineering Department, University of Utah, Salt Lake City, UT, USA, and in 1985 the Electrical and Computer Engineering Department, University of Colorado, Boulder, CO, USA, as a Visiting Researcher in the field of microwave bioelectromagnetics. From 1990 to 1998, she was with the Department of Electrical Engineering, University of Palermo, Palermo, Italy, as an Assistant Professor. In 1998, she joined the University of Messina, Messina, Italy, as an Associate Professor of electronics and became the head of the Microwave Electronics (ELEMIC) Lab. Her current research interests are in the field of temperature-dependent linear and noise characterization techniques for solid-state devices, cryogenic measurements and modeling of field-effect transistors and high-electron mobility transistors, noise modeling of bipolar transistors and FETs hybrid microwave integrated circuit and monolithic microwave integrated circuit design, neural network and genetic algorithm modeling of devices, design and realization of hybrid low-noise circuits based on either conventional and super-conductive materials, characterization and modeling of thin-film sensors. She has authored or coauthored more than 200 papers published on international journals as well as in proceedings of international conferences.

Prof. Caddemi serves as an associate editor of the *International Journal of Numerical Modelling: Electronic Networks, Devices and Fields*. She is also a member of the editorial board of *Microwave Review*, a publication of the Serbia and Montenegro IEEE Microwave Theory and Techniques Society (MTT-S) Chapter and the Serbian national Society for Microwave Technique, Technologies and Systems. She serves as Chair for the IEEE International Workshop on Integrated Nonlinear Microwave and Millimetre-wave Circuits (INMMiC), Taormina, Italy, 2015.

Giorgio Vannini (S'87–M'92) received the Laurea degree in electronic engineering and Ph.D. degree in electronic and computer science engineering from the University of Bologna, Bologna, Italy, in 1987 and 1992, respectively.

In 1992, he joined the Department of Electronics, University of Bologna, Bologna, Italy, as a Research Associate. From 1994 to 1998, he was also with the Research Centre on Electronics, Computer Science and Telecommunication Engineering, National Research Council (CSITE), Bologna, where he was responsible for MMIC testing and the Computer-Aided Design (CAD) Laboratory. In 1998, he joined the University of Ferrara, Ferrara, Italy, as an Associate Professor, where, since 2005, he has been a Full Professor of electronics. He is currently the Head of the Engineering Department, University of Ferrara. During his academic career, he has been a teacher of applied electronics, electronics for communications, and industrial electronics. He is a cofounder of the academic spin-off Microwave Electronics for Communications (MEC). He has coauthored over 200 papers devoted to ED modeling, computer-aided design techniques for monolithich microwave integrated circuits, and nonlinear circuit analysis and design.

Dr. Vannini is a member of the Gallium Arsenide Application Symposium (GAAS) Association.

Dominique M. M.-P. Schreurs (S'90–M'97–SM'02–F'12) received the M.Sc. degree in electronic engineering and Ph.D. degree from the University of Leuven (KU Leuven), Leuven, Belgium.

She is currently a Full Professor with KU Leuven, Leuven, Belgium. She has been a Visiting Scientist with Agilent Technologies, Eidgenössische Technische Hochschule Zürich (ETH Zürich), and the National Institute of Standards and Technology (NIST). Her main research interests concern the (non)linear characterization and modeling of active microwave devices, and (non)linear hybrid and integrated circuit design for telecommunications and biomedical applications.

Prof. Schreurs is serving on the AdCom of the IEEE Microwave Theory and Techniques Society (MTT-S). She is an MTT Distinguished Microwave Lecturer. She is an editor of the IEEE TRANSACTIONS ON MICROWAVE THEORY AND TECHNIQUES and past chair of the MTT-S Educational Committee. She also serves on the Executive Committee of the ARFTG organization and was general chair of the 2007 and 2012 Spring ARFTG Conference. She was also cochair of the European Microwave Conference in 2008.